# Structural Basis for the Metal-Selective Activation of the Manganese Transport Regulator of *Bacillus subtilis*[†,‡]

Joseph I. Kliegman,[§] Sarah L. Griner,[§] John D. Helmann,[∥] Richard G. Brennan,[⊥] and Arthur Glasfeld*[,§]

*Department of Chemistry, Reed College, Portland, Oregon 97202, Department of Microbiology, Wing Hall, Cornell University, Ithaca, New York 14853, and Department of Biochemistry and Molecular Biology, University of Texas M. D. Anderson Cancer Center, Unit 1000, Houston, Texas 77030*

*Received November 27, 2005; Revised Manuscript Received January 2, 2006*

ABSTRACT: The manganese transport regulator (MntR) of *Bacillus subtilis* is activated by $Mn^{2+}$ to repress transcription of genes encoding transporters involved in the uptake of manganese. MntR is also strongly activated by cadmium, both in vivo and in vitro, but it is poorly activated by other metal cations, including calcium and zinc. The previously published MntR·$Mn^{2+}$ structure revealed a binuclear complex of manganese ions with a metal−metal separation of 3.3 Å (herein designated the AB conformer). Analysis of four additional crystal forms of MntR·$Mn^{2+}$ reveals that the AB conformer is only observed in monoclinic crystals at 100 K, suggesting that this conformation may be stabilized by crystal packing forces. In contrast, monoclinic crystals analyzed at room temperature (at either pH 6.5 or pH 8.5), and a second hexagonal crystal form (analyzed at 100 K), all reveal the shift of one manganese ion by 2.5 Å, thereby leading to a newly identified conformation (the AC conformer) with an internuclear distance of 4.4 Å. Significantly, the cadmium and calcium complexes of MntR also contain binuclear complexes with a 4.4 Å internuclear separation. In contrast, the zinc complex of MntR contains only one metal ion per subunit, in the A site. Isothermal titration calorimetry confirms the stoichiometry of $Mn^{2+}$, $Cd^{2+}$, and $Zn^{2+}$ binding to MntR. We propose that the specificity of MntR activation is tied to productive binding of metal ions at two sites; the A site appears to act as a selectivity filter, determining whether the B or C site will be occupied and thereby fully activate MntR.

Manganese is essential to all forms of life. By virtue of its ability to participate in Lewis acid catalysis and redox chemistry, manganese contributes to a broad array of enzymatic functions (*1*). In plants, a manganese-containing cofactor is at the heart of the oxygen-evolving complex (*2*), and in mammals, a manganese-dependent superoxide dismutase helps to protect mitochondria from the byproducts of aerobic metabolism (*3*). In bacteria, manganese also performs these functions, and it plays a significant role in the virulence of several pathogens (*4*−*6*). Despite its contributions to cellular chemistry, manganese becomes toxic at elevated concentrations. Workers overexposed to manganese may experience a behavioral disorder known as "manganese madness" and suffer damage to motor neurons (*7*). An excess of manganese can also be toxic to bacteria (*5*, *8*, *9*). Thus, the health of the organism requires both the ability to acquire manganese from the environment and the capacity to block uptake when cellular concentrations become excessive.

The *Bacillus subtilis* manganese transport regulator (MntR)[1] is the prototype for a subgroup of proteins from the DtxR/IdeR superfamily that respond to $Mn^{2+}$ rather than $Fe^{2+}$ (*8*). Subsequent studies have revealed MntR orthologues in several other bacterial species (*10*−*14*). When activated by $Mn^{2+}$, MntR binds to its operators to block expression of manganese transport systems encoded by the *mntABCD* and *mntH* operons (*8*, *9*). A *B. subtilis* mutant lacking a functional *mntR* gene is unusually sensitive to extracellular manganese and shows reduced growth on medium containing just 3 $\mu$M $Mn^{2+}$ (*8*). Characterization of MntR in vivo and in vitro (*8*, *15*−*17*) has shown that it is highly selective for $Mn^{2+}$ as an effector; DNA-binding activity is distinctly diminished in the presence of other metal cations including $Mg^{2+}$, $Ca^{2+}$, $Fe^{2+}$, $Co^{2+}$, $Ni^{2+}$, and $Zn^{2+}$. However, $Cd^{2+}$ activates MntR as well as, or better than, $Mn^{2+}$ (*8*, *16*, *17*). A nonessential metal cation, $Cd^{2+}$ is a threat to cellular health. In bacteria and humans, cadmium is taken up adventitiously by manganese transporters (*5*, *18*), and cadmium sensitivity is enhanced in an *mntR* null mutant of

[†] This work was supported in part by NIH Grant GM069644 (to A.G.) and NIH Grant GM059323 (to J.D.H.). Purchase of the isothermal titration microcalorimeter was made possible by NSF Grant CHE-0321336.

[‡] Crystallographic data and coordinates have been deposited in the RCSB Protein Data Bank under the file names 2EV0, 2EV5, 2EV6, 2F5C, 2F5D, 2F5E, and 2F5F.

* To whom correspondence should be addressed. Telephone: (503) 517-7679. Fax: (503) 788-6643. E-mail: glasfeld@reed.edu.

[§] Reed College.

[∥] Cornell University.

[⊥] University of Texas M. D. Anderson Cancer Center.

[1] Abbreviations: MntR, manganese transport regulator; D8M, MntR containing the Asp8 to Met mutation; DtxR, diphtheria toxin repressor; HEPES, 4-(2-hydroxyethyl)piperazine-1-ethanesulfonic acid; Tris, tris-(hydroxymethyl)aminomethane; MES, 4-morpholinoethanesulfonic acid; PEG, poly(ethylene glycol); HTH, helix−turn−helix; RMSD, root mean square deviation; ITC, isothermal titration calorimetry.

10.1021/bi0524215 CCC: $33.50 
Published on Web 02/24/2006

*B. subtilis* (*8*). The activation of MntR by $Cd^{2+}$ blocks expression of proteins inadvertently responsible for the uptake of cadmium, suggesting that cadmium is a second biologically relevant activator of MntR.

In the past few years, a number of biochemical and structural studies have begun to elucidate the sources of metal specificity in a variety of metal ion dependent transcriptional regulators (*19*). As examples, the structures of metal-bound forms of NikR (*20*), CueR, and ZntR (*21*) point to a combination of factors, including coordination number, geometry, and charge complementarity. In an extreme example of metal ion selectivity, CueR binds its cognate effector $Cu^{+}$ with zeptomolar ($10^{-21}$) affinity, while showing no activation by $Zn^{2+}$ at concentrations up to 1 mM (*21*). Analyses of metalloregulators of the SmtB/ArsR family reveal that selective metal responses require binding sites finely tuned to respond to the ambient metal ions within the cell; some metals do not elicit genetic responses simply because they are present in the cytosol at concentrations too low to trigger a response. Conversely, other metals can bind to the regulator but fail to elicit a response due to an altered coordination number or geometry (*22*).

Within the diphtheria toxin repressor (DtxR) superfamily, *Corynebacterium diphtheriae* DtxR and the *Mycobacterium tuberculosis* iron-dependent repressor (IdeR) have been crystallized in the presence of various metal ion effectors, revealing two metal-binding sites per subunit, separated by over 9 Å (*23*−*25*). DtxR discriminates against 5 mM $Mn^{2+}$ in the site responsible for effecting the $Fe^{2+}$-dependent allosteric change that activates DtxR for DNA binding (*26*, *27*). Guedon and Helmann have shown that modifications to sulfur-containing ligands, replacing Cys102 with glutamate or Met10 with aspartate, generate a mutant DtxR that is strongly activated by $Mn^{2+}$ in *B. subtilis* cells (*15*), indicating that ligand selection plays a role in allowing DtxR to discriminate against the noncognate metal ion manganese.

MntR demonstrates the opposite selectivity in vivo and in vitro, responding selectively to $Mn^{2+}$ over $Fe^{2+}$, despite being a homologue of DtxR (*8*, *15*, *17*). Ligand selection was initially hypothesized to be responsible for this selectivity. Unlike DtxR, MntR has no sulfur-containing residues in metal-binding positions. Indeed, it is possible to relax the specificity of MntR with respect to $Fe^{2+}$ by mutation of the metal-binding residue, Asp8, to methionine, which replaces a carboxylate side chain with a thioether group. The resulting MntR mutant, D8M, is better activated by $Fe^{2+}$ in vivo than wild-type MntR (*15*).

To develop a better understanding of the structural origins of metal ion selectivity in MntR, we determined the X-ray crystal structures of wild-type MntR and the D8M mutant bound to $Mn^{2+}$ (*28*). Wild-type MntR, like DtxR, binds two metal ions per subunit of the active homodimer. However, the metal ion geometry for this ion pair is substantially different than that observed in DtxR, with the metal ions bound at a distance of 3.3 Å (*28*). Manganese ions occupying the two sites, labeled A and B, lie at the interface of two domains: an N-terminal DNA-binding domain (residues 2−70) and a C-terminal dimerization domain (residues 71−142; Figure 1). Our hypothesis for the selectivity of MntR for $Mn^{2+}$ over $Fe^{2+}$ noted the unusual, pseudo-heptacoordinate geometry of the A site, with seven protein and solvent ligands within 2.6 Å of the manganese ion (*28*). When the B site is disrupted by the D8M mutation, the A site collapses to a lower coordination number, and the selectivity of MntR for $Mn^{2+}$ over $Fe^{2+}$ is compromised (*15*, *17*).

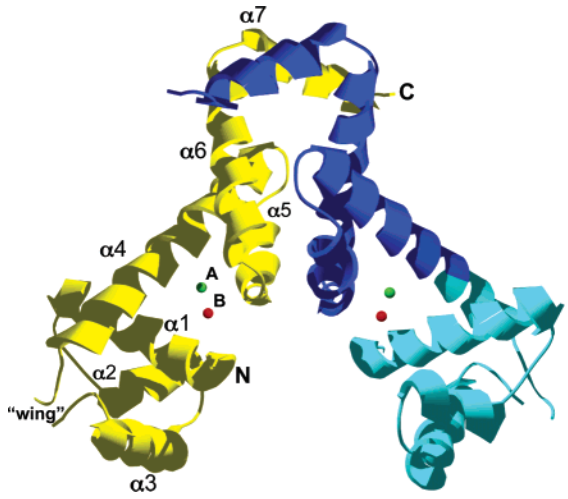


FIGURE 1: Structure of the MntR dimer bound to $Mn^{2+}$ (*28*). One subunit is colored yellow and the second is blue, with the dimerization domain in dark blue and DNA-binding domain in turquoise. The A-site manganese ions are in green, and the B-site manganese ions are in red. The N- and C-termini are labeled for the yellow subunit, as are the secondary structure elements.

To further describe the structural origins of metal ion selectivity in MntR, we present here a crystallographic and thermodynamic study of MntR binding to $Mn^{2+}$, $Cd^{2+}$, $Ca^{2+}$, and $Zn^{2+}$. Significantly, we now find that $Mn^{2+}$, $Cd^{2+}$, and $Ca^{2+}$ all generate a novel binuclear complex in which the B site is vacant and the second ion occupies a new site to generate a binuclear complex (the AC conformer) with a 4.4 Å internuclear distance. The AB and AC conformers use the same set of protein ligands to bind metals but differ in side chain conformations and the additional involvement of one backbone oxygen in conformer AC. Thus, MntR is flexible in its metal-binding geometry. Comparison of the biologically active $Mn^{2+}$ and $Cd^{2+}$ complexes with the inactive, mononuclear $Zn^{2+}$ complex suggests that both geometry and ligand selection contribute to selectivity. The A site appears to act as a selectivity filter that controls occupancy of the second site, which is essential for full activation of MntR for DNA binding.

## EXPERIMENTAL PROCEDURES

*Protein Expression and Purification.* Wild-type MntR was expressed and purified from recombinant *Escherichia coli* as described previously (*28*). MntR solutions (10−14 mg/mL) to be used for crystallization were dialyzed extensively against 25 mM HEPES, pH 7.5, containing 200 mM NaCl and 10% glycerol, with 10 g/L Chelex resin added to the final exchange of buffer. In preparation for isothermal titration calorimetry (ITC), MntR solutions were dialyzed against 25 mM Tris·HCl, pH 8.0, containing 500 mM NaCl and 10% glycerol. The final exchange of buffer included 10 g/L Chelex resin.

*Crystallization and Data Collection.* All crystals were grown using the hanging drop vapor diffusion method, with equal volumes of protein and well solutions added to the drop. The MntR·$Cd^{2+}$ complex was crystallized under conditions similar to those reported for the MntR·$Mn^{2+}$

Table 1: Crystallization Conditions for Metal Complexes of MntR Reported in This Study

| structure/PDB ID | buffer | precipitant | metal/salt | temp (K)/ cryoprotectant |
|---|---|---|---|---|
| MntR·$Mn^{2+}$, AC conf, pH 6.5/2F2D | 100 mM MES | 15% PEG 4000 | 2 mM $MnCl_2$/80 mM $CaCl_2$ | 295 |
| MntR·$Mn^{2+}$, AB conf, pH 6.5/2F5E | 100 mM sodium cacodylate | 15% PEG 4000 | 2 mM $MnCl_2$/100 mM $MgCl_2$ | 100/20% glycerol |
| MntR·$Mn^{2+}$, AC conf, pH 8.5/2F5F | 100 mM Tris·HCl | 25% PEG 400 | 2 mM $MnCl_2$/200 mM $Li_2SO_4$ | 295 |
| MntR·$Mn^{2+}$, hexagonal, pH 8.5/2F5C | 100 mM Tris·HCl | 25% PEG 400 | 2 mM $MnCl_2$/120 mM $Li_2SO_4$ | 100/10% glycerol |
| MntR·$Cd^{2+}$, pH 8.5/2EV0 | 100 mM Tris·HCl | 15% PEG 400 | 0.5 mM $CdCl_2$/200 mM $Li_2SO_4$ | 100/35% PEG 400 |
| MntR·$Ca^{2+}$, pH 8.0/2EV5 | 100 mM Tris·HCl | 18% PEG 8000 | 200 mM calcium acetate | 100/20% glycerol |
| MntR·$Zn^{2+}$, pH 7.0/2EV6 | 100 mM sodium citrate | 20% PEG 3000 | 5 mM $ZnCl_2$/200 mM triammonium citrate | 100/20% glycerol |

Table 2: Data and Refinement Statistics for Structures of Metal Complexes with MntR

| | MntR·$Mn^{2+}$, pH 6.5, conf AC | MntR·$Mn^{2+}$, pH 6.5, conf AB | MntR·$Mn^{2+}$, pH 8.5, conf AC | MntR·$Mn^{2+}$, hexagonal, conf AC | MntR·$Cd^{2+}$, pH 8.5 | MntR·$Ca^{2+}$, pH 8.0 | MntR·$Zn^{2+}$, pH 7.0 |
|---|---|---|---|---|---|---|---|
| data source | R-Axis IV | R-Axis IV | R-Axis IV | ALS 4.2.2 | SSRL 9.2 | ALS 8.2.1 | ALS 8.2.1 |
| wavelength (Å) | 1.5418 | 1.5418 | 1.5418 | 1.1271 | 0.9840 | 1.0781 | 1.0781 |
| temp (K) | 295 | 100 | 295 | 100 | 100 | 100 | 100 |
| space group | $P2_1$ | $P2_1$ | $P2_1$ | $P6_522$ | $P2_1$ | $P2_1$ | $P2_1$ |
| *a* (Å) | 50.7 | 49.4 | 50.6 | 41.3 | 48.9 | 49.7 | 49.7 |
| *b* (Å) | 46.4 | 46.0 | 46.4 | 41.3 | 46.2 | 45.8 | 46.0 |
| *c* (Å) | 75.8 | 74.4 | 75.4 | 301.4 | 74.9 | 74.7 | 74.4 |
| $\beta$ (deg) | 94.6 | 94.3 | 94.3 | | 93.0 | 93.8 | 93.2 |
| resolution (Å)[a] | 31.50−1.90 (2.02−1.90) | 20.0−2.20 (2.34−2.20) | 31.7−2.40 (2.55−2.40) | 20.0−2.40 (2.4−2.49) | 39.95−1.65 (1.75−1.65) | 39.01−2.00 (2.00−2.13) | 37.14−1.70 (1.81−1.70) |
| no. of reflections | | | | | | | |
| total | 57546 | 40735 | 29487 | 104036 | 88240 | 50943 | 74441 |
| unique | 25228 | 16728 | 13217 | 5943 | 37469 | 21041 | 34860 |
| completeness | 90.0 (61.1) | 97.3 (97.1) | 95.0 (93.8) | 88.1 (48.9) | 92.6 (90.7) | 91.8 (91.4) | 93.6 (72.1) |
| $I/\sigma(I)$ | 6.2 (2.5) | 7.7 (2.2) | 5.2 (2.0) | 19.8 (6.6) | 8.4 (3.7) | 4.4 (2.4) | 5.6 (2.2) |
| $R_{merge}$ (%)[b] | 6.4 (27.0) | 8.3 (32.5) | 8.7 (34.2) | 9.6 (32.3) | 4.8 (19.5) | 10.9 (27.8) | 7.7 (32.8) |
| no. of protein atoms | 2147 | 2154 | 2238 | 1164 | 2154 | 2165 | 2261 |
| no. of metal ions | 4 | 4 | 4 | 2 | 5 | 4 | 2 |
| no. of solvent atoms | 87 | 69 | 37 | 8 | 262 | 89 | 214 |
| no. of solute atoms | 0 | 0 | 0 | 10 | 0 | 0 | 3 |
| $R_{cryst}/R_{free}$ (%)[c] | 21.0/23.0 (29.5/31.1) | 23.7/28.6 (30.1/35.1) | 22.2/25.7 (26.6/33.4) | 24.8/30.3 (29.9/40.2) | 20.7/22.9 (26.0/28.4) | 24.8/29.1 (30.8/33.8) | 23.3/26.0 (31.4/36.2) |
| bond length deviation (Å) | 0.004 | 0.006 | 0.006 | 0.007 | 0.005 | 0.006 | 0.005 |
| bond angle deviation (deg) | 0.98 | 1.0 | 1.1 | 1.20 | 1.0 | 1.0 | 1.0 |
| average *B*-factor | 36.4 | 34.7 | 43.7 | 45.2 | 28.3 | 31.9 | 26.8 |

[a] Numbers in parentheses reflect the highest resolution shell. [b] $R_{merge} = \sum_h\sum_j|I_{h,j} - \langle I_h\rangle|/\sum_j\sum_h|I_{h,j}|$, where $I_{h,j}$ is the *j*th observation of reflection *h*. [c] $R_{cryst} = \sum_h||F_o| - |F_c||/\sum_h|F_o|$, where $F_o$ and $F_c$ are the observed and calculated structure factors for reflection *h*. $R_{free}$ is calculated similarly for 5−10% of the data not used in refinement.

complex (Table 1; *28*), except that 500 $\mu$M $CdCl_2$ replaced 2 mM $MnCl_2$ in the well solution. Other conditions were developed from broad crystallization screens containing the metal ion of interest. Crystals of the MntR·$Mn^{2+}$ complex in a hexagonal space group were obtained from mixtures containing 23 base pair duplex DNA containing the *mntH* operator sequence, 5′-GTAATTTGCCTTAAGGAAACTCC, but DNA did not cocrystallize with MntR (Table 1). Data collection was performed using an R-Axis IV imaging plate system coupled to a Rigaku RU300 rotating anode generator providing Cu Kα radiation and several synchrotron sources (Table 2). Low-temperature data were collected from crystals equilibrated with solutions containing cryoprotectants (Table 1) that were flash-cooled by placing the crystals in a flow of nitrogen gas cooled to 100 K. The data were processed using MOSFLM (*29*) or D*Trek (*30*) and scaled using the SCALA program implemented in the CCP4 suite of crystallographic analysis software (*31*).

*Structure Determination and Refinement.* The structure of MntR from the previously reported MntR·$Mn^{2+}$ complex (PDB ID 1ON1; *28*) was used, without bound metal ions, as a search model to obtain molecular replacement solutions for each crystal form using CNS (*32*). Subsequent refinement proceeded with a random set of 5−10% of the crystallographic data set aside for cross-validation. Metal ions were added to the model after rigid body refinement of the original molecular replacement solution, using $\sigma_A$-weighted $F_o - F_c$ maps as a guide. Anomalous Fourier difference maps using calculated phases were used, when possible, to confirm the identity of bound metals. The anomalous signal of manganese is strong when using Cu Kα radiation and can be used to readily distinguish manganese from calcium and magnesium ions also present in the crystallization buffer (*33*). Also, a data set was collected from a crystal of the MntR·$Zn^{2+}$ complex at the zinc X-ray absorption edge in order to verify placement and identity of the bound zinc ions. In the final rounds of refinement solvent and solute molecules were added where residual electron density in $\sigma_A$-weighted $F_o - F_c$ maps exceeded 3$\sigma$ and reasonable stereochemistry was observed. The stereochemical quality of the models was evaluated by PROCHECK (*32*). Crystallographic data and the models reported here have been deposited in the RCSB Protein Data Bank (PDB ID 1EV0, 1EV5, 1EV6, 2F5C, 2F5D, 2F5E, and 2F5F).

*Isothermal Titration Calorimetry.* Calorimetric titrations of MntR with metal ions were performed on a MicroCal VP-ITC instrument (Northampton, MA). The sample cell was held at 25 °C. Metal ion salts and protein were dissolved in 25 mM Tris·HCl, pH 8.0, 500 mM NaCl, and 10% glycerol. The high salt concentration was necessary to maintain the solubility of the MntR−metal ion complexes during the titration. Typical protein concentration, determined by UV absorbance at 280 nm (*16*), was 30−100 $\mu$M in MntR subunits, and metal ion concentration in the injector was typically 7−20-fold higher (depending on the number of binding sites detected). Solutions were degassed for 5−10 min prior to use. After an initial addition of 4 $\mu$L of metal ion solution, all subsequent additions were 8 $\mu$L with 180 s intervals between additions. Background data were collected by titrating metal ion solutions into buffer alone and were subtracted from data obtained with MntR present. Titration data were fit assuming independent interaction of each MntR monomer with the metal ions of interest. Titration data were analyzed using Origin 7.0 software (OriginLab, Northampton, MA) and tested with models provided by the instrument manufacturer that describe a single site per monomer, two sequential binding sites, and two noninteracting binding sites.

*Fluorescence Anisotropy.* The DNA-binding activity of MntR was measured using fluorescence anisotropy (*35*). A 5′-fluoresceinated 21-base oligodeoxynucleotide with the sequence GAGTTTCCTTAAGGCAAATTG, which contains the *mntH* operator sequence, was annealed with a 10% molar excess of its complement at 80 °C for 10 min to create a fragment of duplex DNA with a single fluorescein label. Binding was measured by titrating solutions of MntR into 1 mL of solution containing labeled DNA (1 nM) in 25 mM Tris·HCl, in the presence or absence of 1 mM $MnCl_2$, and 300 mM NaCl, 100 mM $CaCl_2$, or 100 mM $MgCl_2$. Anisotropy was measured on a Beacon 2000 fluorescence polarization instrument (Panvera, Madison, WI). Data were analyzed assuming a 1:1 binding stoichiometry between the MntR dimer and labeled DNA.

## RESULTS

*Crystallization, Data Collection, and Model Refinement.* All but one of the complexes reported here crystallized in the monoclinic space group $P2_1$ with similar cell parameters (Table 2). The exception is a crystal of the MntR·$Mn^{2+}$ complex grown in the hexagonal space group $P6_522$ from PEG 400 in the presence of a 23 base pair DNA duplex, which did not cocrystallize with the MntR·$Mn^{2+}$ complex. In monoclinic crystals, the asymmetric unit contains two MntR subunits in the biologically active, dimeric form of the protein. In the hexagonal crystal form, a single subunit occupies the asymmetric unit, and the active dimer is generated by rotation about a crystallographic 2-fold axis. The protein chain is generally well-defined in the electron density and can be traced from the second or third residue through to or near to the C-terminus, with disorder obscuring placement of the last few residues in most models. In addition, a flexible loop (residues 54−58) connecting the two $\beta$-strands that form the "wing" in the winged helix−turn−helix DNA-binding motif (*36*) is often unrepresented in electron density maps. This loop is visible in the MntR·$Zn^{2+}$ complex, the room temperature structure of MntR·$Mn^{2+}$ at pH 8.5, and the hexagonal MntR·$Mn^{2+}$ complex but is omitted from the other models. Refinement of all models included bound metal ions and solvent molecules yielding excellent geometry and agreement with the crystallographic data (Table 2).

*Tertiary Structure of Metal Ion Complexes with MntR.* There is extensive similarity among the structures described here. Regardless of the bound metal ion or crystallization conditions, MntR adopts a common fold, with an N-terminal 70-residue DNA-binding domain, containing a winged helix−turn−helix motif, and a C-terminal dimerization domain, comprising residues 71−142. The two domains are connected by a 23-residue helix ($\alpha$4, residues 64−86) that reaches from the wing of the DNA-binding motif to the dimer interface. Among the different MntR−metal ion complexes, the dimeric C-terminal domains show virtually no structural variation. Root mean square deviations in the positions of the $C_\alpha$ atoms of dimers of the C-terminal domain are universally less than 0.36 Å. There is somewhat greater variation in the positions of the DNA-binding domains with respect to the dimerization domain, which leads to a maximum RMSD between $C_\alpha$ atoms for the entire dimer of 1.20 Å. While the DNA-binding domain retains a constant fold, except for the flexible loop and the first four to five residues, it can shift in position via motion centered on the backbone of residues 66−71, at the base of helix $\alpha$4. The twisting motion that takes place has the effect of slightly altering the separation of the symmetry-related recognition helices that are presumed to interact in the major groove of DNA duplexes containing *mnt* operator sequences (see below).

*Two Alternative Conformations of $Mn^{2+}$ Binding in MntR·$Mn^{2+}$ Complexes.* In the published structure of the MntR·$Mn^{2+}$ complex, MntR binds two manganese ions per subunit in a binuclear complex (Figure 2A; *28*). The two sites, labeled A and B, are separated by 3.3 Å, and the manganese ions are bridged three groups: Glu11 in a $\mu$-1,3 fashion, Glu102, which bridges with a single oxygen atom, and a solvent molecule that we have labeled W1. The high pH of the original crystallization conditions raises the possibility that W1 exists as a $\mu$-hydroxo ligand and could be protonated at a lower pH (*37*). To investigate the potential effects of pH, new crystallization conditions were developed at pH 6.5. The MntR·$Mn^{2+}$ complex again crystallized in the monoclinic space group $P2_1$. When flash-cooled prior to data collection, crystals grown at pH 6.5 contain a structure virtually identical to that previously observed at pH 8.5. The coordination sphere of the A site is completed by the side chains of His77 and Glu99, which each interact as monodentate ligands, a solvent molecule, and the nonbridging carboxylate oxygen of Glu102. The B-site $Mn^{2+}$ is coordinated by the side chain groups of Asp8 and His103, as well as a solvent ligand, which combine with the bridging ligands to create roughly octahedral geometry.

While pH does not affect the conformation of manganese binding in cryocooled crystals of MntR·$Mn^{2+}$, temperature does. A novel pattern of metal binding was revealed in a large crystal of the MntR·$Mn^{2+}$ complex grown at pH 6.5 and mounted at 295 K for data collection. In the new conformation, the two manganese ions are separated by 4.4 Å, as opposed to the 3.3 Å separation observed in the low-temperature structure. The A-site manganese retains its position in both conformations, but at 295 K a novel binding

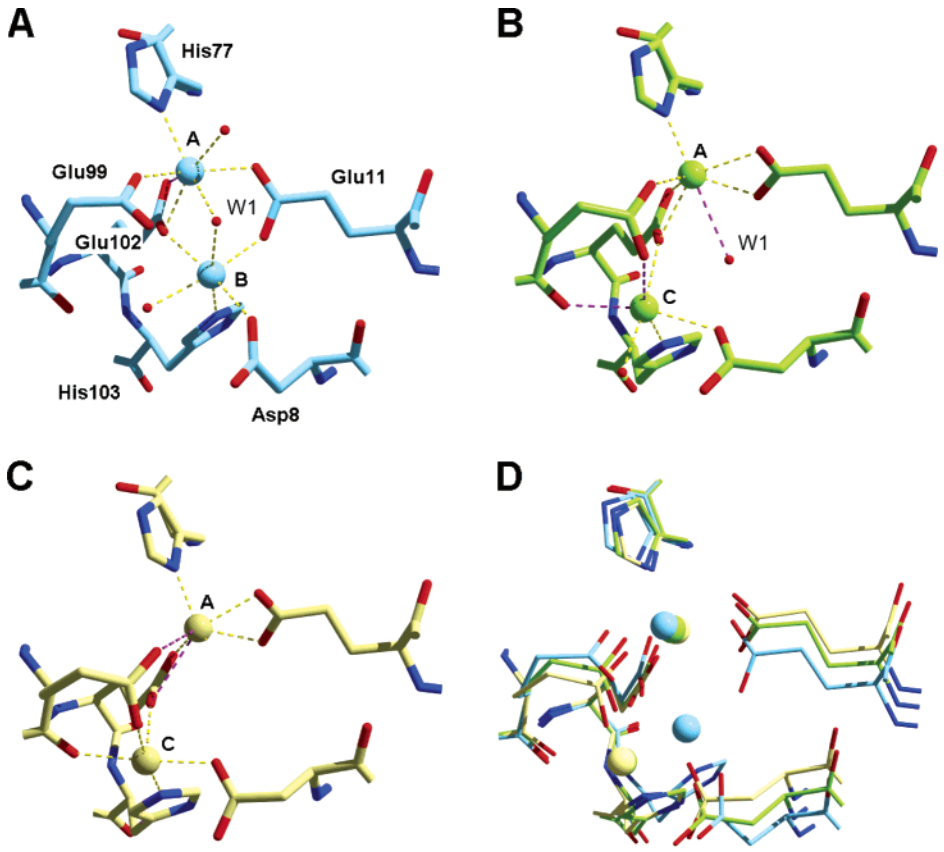


FIGURE 2: Structures of $Mn^{2+}$ complexes with MntR. (A) Conformer AB from monoclinic crystals grown at pH 8.5 and cooled to 100 K. Carbons and $Mn^{2+}$ ions are colored turquoise (*28*). (B) Conformer AC from monoclinic crystals grown at pH 6.5 and held at 295 K. Carbons and $Mn^{2+}$ ions are colored green. (C) Conformer AC from hexagonal crystals grown at pH 8.5 and cooled to 100 K. Carbons and $Mn^{2+}$ ions are colored yellow. (D) Overlay of the three structures. Metal−side chain interactions between 2.5 and 2.8 Å are shown as purple dashed lines in panels A−C.

site, labeled C, is occupied by the second $Mn^{2+}$ 2.5 Å away from the now vacant B site. We distinguish the two conformations with the labels AB and AC to denote the sites occupied by the two metal ions. Upon further investigation, it was determined that the AC conformation is also observed in crystals grown at pH 8.5, when data collection is conducted at 295 K. In an additional experiment (data not shown) we found that equilibration of crystals with cryoprotectant followed by data collection at room temperature also captures the MntR·$Mn^{2+}$ complex in the AC conformation.

The interconversion between the AB and AC conformations is accompanied by significant reorganization of the metal-binding residues in MntR, centered around the ligands that bridge the two metals in both conformations. In the AB conformation, Glu11, Glu102, and the solvent molecule, W1, are bridging, while in conformer AC, the manganese ions are bridged by Glu99 and Glu102. While the side chain carboxylate Glu99 interacts with the A-site metal as a monodentate ligand in the AB conformation, at 295 K it forms a $\mu$-1,3 bridge between the two metal ions through its side chain carboxylate. The side chain of Glu11, which bridges in a $\mu$-1,3 fashion in conformer AB, interacts as a bidentate ligand to the A-site metal in conformer AC (Figure 2).

In conformer AC, the A-site metal has retained an expanded coordination sphere observed previously in crystals cooled to 100 K (*28*). The geometry of the A site in the AB conformation can be described as pseudo-heptacoordinate, reflecting its distorted octahedral geometry with an additional longer range interaction (2.6 Å) to a seventh ligand, O$\epsilon$1 of Glu102. The side chains of His77 and Glu102 bond similarly to the A-site metal in both conformations, but the nonbridging solvent molecule seen in conformation AB is absent in the AC conformation, essentially replaced by a second interaction with Glu11. The bridging solvent molecule in conformer AB, W1, is retained as a ligand by the $Mn^{2+}$ in site A (Figure 2B). While the position of W1 is somewhat dynamic in the AC conformation, varying between 2.3 and 2.9 Å in the two room temperature structures (Table 3), the electron density for that water molecule is clearly visible in $F_o - F_c$ omit electron density maps at 5$\sigma$ above background. The other metal−ligand distances range from 1.95 to 2.62 Å (Table 3).

The C site occupied in conformer AC lacks interactions with Glu11 and the $\mu$-aquo/hydroxo bridging ligand of conformer AB but is compensated by interactions with the side chain carboxylate of bridging residue Glu99 and its backbone oxygen. The side chain positions of Asp8 and His103 are altered slightly in the higher temperature conformation but remain bonded to the metal in site C and, along with a solvent ligand, sustain octahedral coordination to the manganese ion.

Although temperature determines the metal-binding conformation in monoclinic crystals of the MntR·$Mn^{2+}$ complex, its influence does not extend to the hexagonal crystal form of manganese-bound MntR. In those crystals, cooled to 100 K for data collection, conformer AC predominates despite

Table 3: Table of Metal−Ligand Distances (in Å) and Metal−Metal Distance for MntR−Metal Ion Complexes[a]

| | $Mn^{2+}$ conf AB, pH 8.5, 100 K,[b] *pH 6.5, 100 K* | | $Mn^{2+}$ conf AC, pH 8.5, 295 K, *pH 6.5, 295 K* | | $Cd^{2+}$ | | $Ca^{2+}$ | | $Zn^{2+}$ | |
|---|---|---|---|---|---|---|---|---|---|---|
| | subunit 1 | subunit 2 | subunit 1 | subunit 2 | subunit 1 | subunit 2 | subunit 1 | subunit 2 | subunit 1 | subunit 2 |
| A site | | | | | | | | | | |
| Glu11 Oϵ1, Oϵ2 | na,[c] 2.19 | na, 2.16 | 2.28, 2.25 | 2.24, 2.21 | 2.48, 2.39 | 2.31, 2.39[d] | 2.61, 2.47 | 2.69, 2.41 | na, 2.06 | na, 1.93 |
| | *na, 2.41* | *na, 2.16* | *2.36, 2.41* | *2.35, 2.49* | | 2.67, 2.40[d] | | | | |
| His77 | 2.20 | 2.18 | 2.19 | 2.13 | 2.33 | 2.26 | 2.41 | 2.36 | 1.98 | 2.01 |
| | *2.22* | *2.11* | *2.13* | *2.12* | | | | | | |
| Glu99 Oϵ2 | 2.19 | 2.21 | 2.05 | 2.13 | 2.26 | 2.28 | 2.27 | 2.18 | 2.59c | 3.00 |
| | *2.12* | *2.14* | *2.22* | *2.19* | | | | | | |
| Glu102 Oϵ1, Oϵ2 | 2.57, 2.25 | 2.60, 2.24 | 2.53, 2.28 | 2.12, 2.62 | 2.44, 2.43 | 2.41, 2.54 | 2.40, 2.58 | 2.43, 2.64 | 2.48, 2.06 | 2.56, 2.04 |
| | *2.51, 2.33* | *2.42, 2.49* | *2.31, 2.41* | *2.31, 2.43* | | | | | | |
| solvent 1[e] | 2.40 | 2.40 | 2.42 | 2.28 | 2.46 | np[f] | 2.33 | 2.21 | na | na |
| | *2.45* | *2.50* | *2.91* | *2.52* | | | | | | |
| solvent 2[g] | 2.35 | 2.40 | np | np | na | na | 2.41 | 2.57 | 2.15 | 2.07 |
| | *2.39* | *2.18* | | | | | | | | |
| B/C site | | | | | | | | | | |
| Asp8 | 2.39 | 2.28 | 2.38 | 2.27 | 2.32 | 2.30 | 2.87, 2.46 | 2.80, 2.48 | | |
| | *2.41* | *2.49* | *2.42* | *2.38* | | | | | | |
| Glu11 | 2.14 | 2.18 | na | na | na | na | na | na | | |
| | *2.22* | *2.30* | | | | | | | | |
| Glu99 Oϵ1, O | na | na | 2.54, 2.61 | 2.43, 2.56 | 2.30, 2.41 | 2.39, 2.38 | 2.61, 2.59 | 2.46, 2.65 | | |
| | | | *2.51, 2.62* | *2.56, 2.32* | | | | | | |
| Glu102 Oϵ2 | 2.14 | 2.23 | 2.53 | 2.22 | 2.30 | 2.26 | 2.34 | 2.38 | | |
| | *2.23* | *2.01* | *2.44* | *2.46* | | | | | | |
| His103 | 2.33 | 2.23 | 2.34 | 2.18 | 2.28 | 2.23 | 2.51 | 2.40 | | |
| | *2.22* | *2.37* | *2.21* | *2.34* | | | | | | |
| solvent 1[e] | 2.45 | 2.50 | na | na | na | na | na | na | | |
| | *2.49* | *2.61* | | | | | | | | |
| solvent 2 | 2.31 | 2.28 | 1.95 | 2.00 | 2.20 | 2.25 | 2.35 | 2.50 | | |
| | *2.36* | *2.41* | *2.30* | *2.16* | | | | | | |
| $M^{2+}$−$M^{2+}$ | 3.29 | 3.37 | 4.25 | 4.40 | 4.31 | 4.34 | 4.41 | 4.47 | | |
| | *3.41* | *3.30* | *4.44* | *4.43* | | | | | | |

[a] Distances for the two $Mn^{2+}$-binding conformers are listed separately, with the structures solved at pH 8.5 and 6.5 listed separately in roman and italic type. [b] From ref *28*. [c] Not applicable, distance >2.80 Å. [d] Two conformations are modeled for the side chain Glu11. [e] Solvent ligand in bridging position or equivalent position in conformer AC. [f] Not present. [g] Position varies between MntR·$Mn^{2+}$, MntR·$Ca^{2+}$, and MntR·$Zn^{2+}$ complexes.

the low temperature. The $Mn^{2+}$ ions are separated by 4.4 Å in the hexagonal crystal form and are in positions virtually identical to those observed at 295 K in monoclinic crystals (Figure 2C). Data from the hexagonal crystals are 88% complete to only 2.7 Å resolution and extend maximally to 2.4 Å (Table 2), so a detailed analysis of metal−bond distances is inadvisable. Nevertheless, there is strong structural similarity in manganese binding between cryocooled hexagonal crystals and room temperature monoclinic crystals of MntR·$Mn^{2+}$, showing that the temperature-dependent shift in metal ion binding is dependent on the crystal-packing environment.

*Domain Movements in the MntR·$Mn^{2+}$ Complex.* The two conformers of the MntR·$Mn^{2+}$ complex observed in monoclinic crystals are associated with observable movement of the DNA-binding domains with respect to the dimer interface. In the original structure of the MntR·$Mn^{2+}$ complex, solved from cryocooled crystals grown at pH 8.5, the distance between the putative DNA recognition helices of the MntR dimer (as measured between the $C_\alpha$ atoms of Lys41 from each subunit) is 30.2 Å. The separation measured in the room temperature structure of MntR, crystallized at pH 8.5, is 31.6 Å. The separation between DNA-binding domains is consistently greater among structures of the MntR·$Mn^{2+}$ complex obtained at room temperature than at 100 K in the monoclinic crystal form. The packing of MntR dimers into the hexagonal unit cell leads to a novel set of crystal packing interactions and accommodates a significantly larger interhelix separation (33.5 Å) than in any of the monoclinic crystals of MntR·$Mn^{2+}$. The difference can be observed in the immediate vicinity of the bound $Mn^{2+}$ ions. The $C_\alpha$ atoms of residues Asp8 and Glu11, on the N-terminal helix of the DNA-binding domain, are shifted about 0.5 Å with respect to the positions in monoclinic crystals at 295 K and over 1 Å from the positions in conformer AB, observed in monoclinic crystals at 100 K (Figure 2C,D).

*MntR·$Cd^{2+}$ Complex.* The structure of the MntR·$Cd^{2+}$ complex contains two cadmium ions in the A and C sites as well as a cadmium ion indicated by a less prominent peak in electron density, visible at 10$\sigma$, located at the dimer interface, bound by symmetry-related His104 residues. Omit electron density and anomalous Fourier difference maps confirm the presence of a cadmium ion at each position, though we have modeled the cadmium ion at the dimer interface at 50% occupancy. The conditions in the crystal are virtually the same as those that favor the AB conformer of MntR·$Mn^{2+}$, but the structure of MntR complexed with $Cd^{2+}$ is nearly identical to that observed for MntR bound to manganese in conformer AC, both globally and locally. A 3.0 Å resolution data set collected from cadmium-containing crystals at room temperature yields a virtually identical structure, with the two cadmium ions separated by 4.4 Å (data not shown). The RMSD between $C_\alpha$ atoms between the AC conformer of the MntR·$Mn^{2+}$ complex and the MntR·$Cd^{2+}$ complex is 0.37 Å, and the metal−protein interactions are conserved in both. However, the number of bound solvent

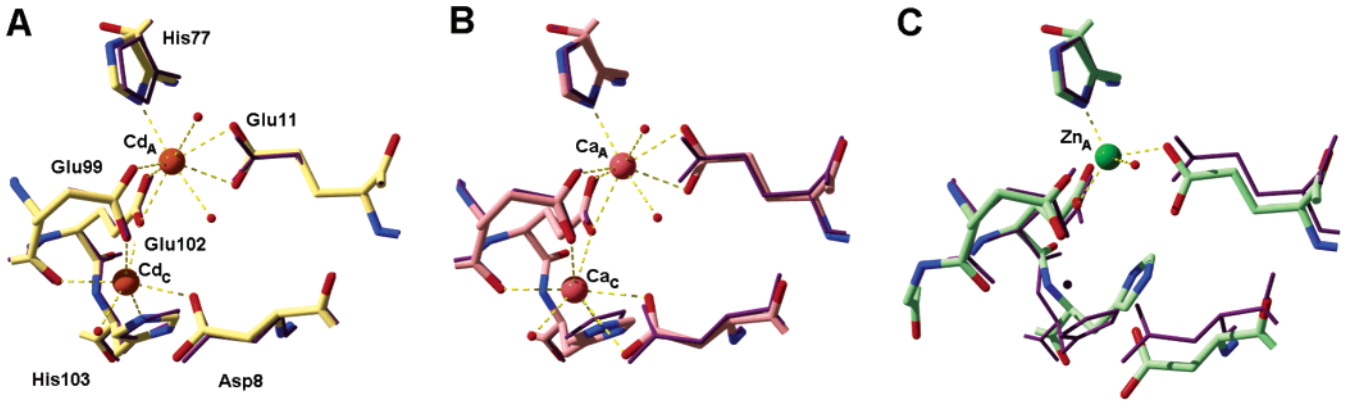


FIGURE 3: Overlays of (A) cadmium, (B) calcium, and (C) zinc complexes of MntR on conformer AC of the MntR·$Mn^{2+}$ complex (in thin purple lines).

ligands in the A site is ambiguous. The electron density for the side chain carboxylate of Glu11 does not correspond to a unique position, even at 1.65 Å resolution, and suggests that Glu11 may interact with the A-site $Cd^{2+}$ in one of two orientations (Figure S1; see Supporting Information). In one of the subunits in the asymmetric unit, Glu11 is modeled as a 50:50 mixture of the two orientations, without a solvent ligand on the A-site $Cd^{2+}$. In the other subunit, the electron density suggests that Glu11 chiefly adopts a single orientation and that W1 resides 2.46 Å from the A-site metal (Figure 3, Table 3). The impact of the disorder associated with the side chain of Glu11 is constrained to W1. The A-site cadmium and all other side chains are well-defined. Although $Cd^{2+}$ has a larger ionic radius in hexacoordinate geometries than high-spin $Mn^{2+}$ (1.09 vs 0.94 Å; *38*), there is no clear trend toward longer metal−ligand bond distances in the MntR·$Cd^{2+}$ complex relative to the MntR·$Mn^{2+}$ complex (Table 3).

*MntR·$Ca^{2+}$ Complex.* The metal−ligand interactions between calcium and MntR are similar to those observed with $Mn^{2+}$ in conformer AC and with $Cd^{2+}$. Calcium ions occupy both the A and C sites, separated by 4.4 Å (Figure 3, Table 3). The identity of the bound $Ca^{2+}$ ions is confirmed by the weak anomalous signal obtained using Cu Kα radiation, which yields peaks of less than 4.5$\sigma$ in the anomalous Fourier difference maps from the MntR·$Ca^{2+}$ complex, in contrast to peaks of 8$\sigma$ or higher obtained from $Mn^{2+}$. In the A site, $Ca^{2+}$ binds in an octacoordinate, roughly square antiprismic geometry with two solvent molecules and six protein ligands (Figure 3). The six protein ligands are bound in similar positions to those adopted in the AC conformation of the MntR·$Mn^{2+}$ and MntR·$Cd^{2+}$ complexes (Figure 3), and one of the solvent molecules is at the W1 position. The second solvent molecule in the calcium A site occupies a position roughly trans to Glu102. (Solvent molecules were likewise observed in this region in the MntR·$Cd^{2+}$ complex, but the distances are greater than 2.8 Å in both subunits, so those solvents are not described as ligands in the cadmium complex.) The C site of the MntR·$Ca^{2+}$ complex retains hexacoordinate geometry as in all other binuclear metal ion complexes of MntR. The metal−ligand distances are generally similar to those observed with either $Mn^{2+}$ or $Cd^{2+}$, ranging from 2.18 to 2.69 Å (Table 3). The interhelix distance between dyadic recognition helices is 31.4 Å and close to that observed for the MntR·$Mn^{2+}$ structure at room temperature, and the overall RMSD between $C_\alpha$ atoms in the manganese (conformer AC) and calcium complexes is 0.31 Å.

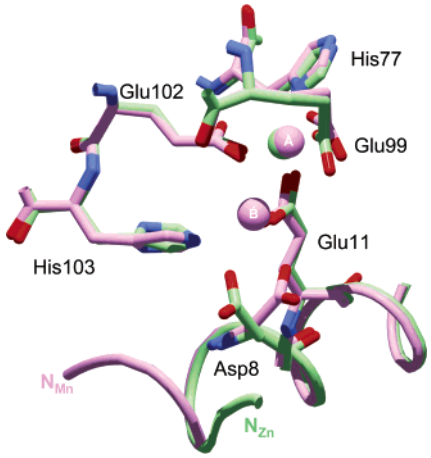


FIGURE 4: The N-terminus of the zinc complex of MntR (green carbon and zinc ion) is unwound with respect to the N-terminus of the MntR·$Mn^{2+}$ complex (purple carbon and manganese ions). The AB conformer of the MntR·$Mn^{2+}$ complex is shown.

*MntR·$Zn^{2+}$ Complex.* Of the four complexes investigated in this study, the MntR·$Zn^{2+}$ structure is unique in containing a single metal ion per MntR subunit, in the A site (Figure 3). While $Mn^{2+}$, $Cd^{2+}$, and $Ca^{2+}$ bind to the A site with geometries that involve six to eight ligands, $Zn^{2+}$ binds with tetracoordinate geometry, accepting metal−ligand bonds from Glu11, His77, Glu102, and a solvent molecule. The second carboxylate oxygen of Glu102 is about 2.5 Å from the zinc ion, but given that the first carboxylate oxygen is found less than 2.1 Å from the zinc (Table 3), the longer interaction is judged to be considerably weaker. The unoccupied C site contains a solvent molecule, hydrogen bonded to the side chain carboxylate of Asp8 and the backbone carbonyl oxygen of Glu99. The absence of a second zinc ion was confirmed by an anomalous Fourier difference map calculated from data collected at the zinc X-ray absorption peak at 1.278 Å.

The failure of zinc to bind in either the B or C sites appears to result from the negative influence of the bound $Zn^{2+}$ in the A site. None of the carboxylate ligands observed to form bridging interactions in other complexes (Glu11, Glu99, and Glu102) are in a position to interact with a metal in the B/C sites. The side chain carboxylate of glutamate 99 is excluded from the coordination sphere of the A-site zinc, which

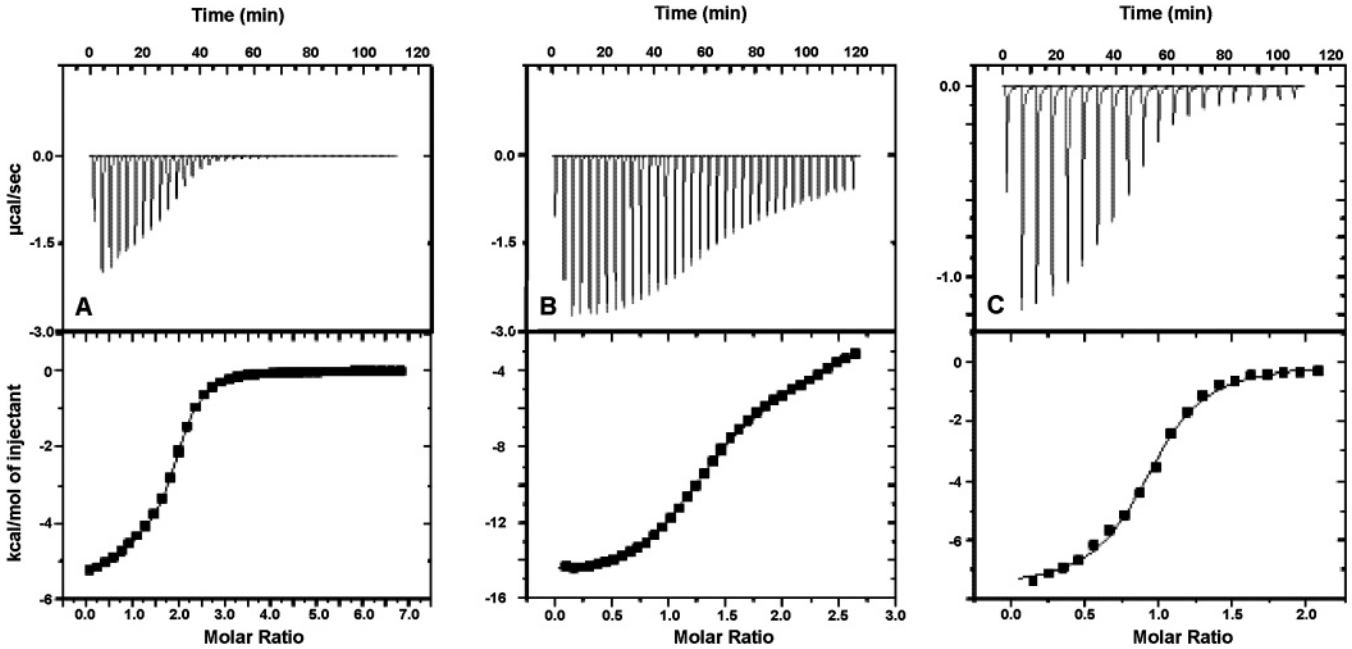


FIGURE 5: Results of isothermal titration calorimetry. (A) Titration of 2.5 mM $MnCl_2$ into a solution of 87 $\mu$M MntR (subunits). (B) Titration of 1.0 mM $CdCl_2$ into 82 $\mu$M MntR. (C) Titration of 0.75 mM $ZnCl_2$ into 38 $\mu$M MntR. Data from the manganese and cadmium titrations were fit with a two-site, sequential binding model, while data from the zinc titration was fit with a single-site model.

removes it from a potential bridging position. Glutamate 11, which is a bridging ligand in the AB conformation, has maintained a position closer to its nonbridging conformation in conformer AC of the MntR·$Mn^{2+}$ complex, reducing its proximity to both the B and C sites. And glutamate 102, which acts as a monodentate bridging carboxylate in the binuclear complexes typically observed in MntR, is significantly reoriented toward the A-site metal. Furthermore, O$\epsilon$1 of Glu102, which does not bond to the zinc, appears to be within hydrogen- bonding distance (3.2 Å) of His103, shifting its position away from both the B and C sites. The ligand geometries are sufficiently perturbed so as to disfavor a second bound zinc ion.

The global conformation of the MntR dimer bound to $Zn^{2+}$ is most similar to conformer AB of the MntR·$Mn^{2+}$ complex. The interhelix separation is 30.7 Å, shorter than that observed in conformer AC in any of the other metal ion complexes. This is reflected in a displacement of residues of Asp8 and Glu11 from the positions observed in conformer AC (Figure 3C). Unlike in the MntR·$Mn^{2+}$ complexes, there is a slight unwinding of the N-terminal helix, on which Asp8 and Glu11 reside, in the zinc complex. Proline 4 in the MntR·$Zn^{2+}$ complex is approximately 6.7 Å from its position in the MntR·$Mn^{2+}$ complex in conformer AB (Figure 4).

*Isothermal Titration Calorimetry.* To confirm the stoichiometry of metal ion binding and to measure affinities of MntR to $Mn^{2+}$, $Cd^{2+}$, $Ca^{2+}$, and $Zn^{2+}$, isothermal titration calorimetry (ITC) was performed. Typical thermograms fit with the sequential binding model are shown in Figure 5. Solutions of each metal ion were titrated into a cell containing MntR at 298 K. Data are taken from three titrations using at least two different protein preparations for each metal ion. The results confirm two-site binding of $Mn^{2+}$ and $Cd^{2+}$ by MntR, with stoichiometries ranging from 1.7 to 2.0 metal ions per subunit. Curve fitting to the titration data does not reliably distinguish between a model describing noncooperative, independent binding of the two metal ions, versus a sequential, cooperative model, but the calculated affinities for the two ions are consistent between the two models. For manganese, the first dissociation constant ranges from 0.2 to 2 $\mu$M, and the second dissociation constant ranges from 5 to 13 $\mu$M. Cadmium gives similar results, with dissociation constants of 2−5 $\mu$M for the first site and 30−60 $\mu$M for the second site. Titration of MntR with $Zn^{2+}$ reveals single-site binding with a dissociation constant of 2−6 $\mu$M and a stoichiometry of binding of 0.9−1.2 zinc ions per MntR subunit (Figure 5C). Titrations of 100 $\mu$M MntR with 2 mM $Ca^{2+}$ failed to reveal a signal.

*DNA Binding in the Presence of Calcium.* The absence of a detectable metal-binding signal with $Ca^{2+}$ in ITC titrations could be attributed either to a lack of detectable enthalpy of binding or to a high dissociation constant. DNA-binding studies monitored by fluorescence anisotropy indicate that weak binding is the cause. MntR, activated by the presence of 1 mM $MnCl_2$, binds to a fluoresceinated 21 base pair fragment of duplex DNA with a dissociation constant of 32 ± 4 nM in 300 mM NaCl (Figure 6). In the absence of $Mn^{2+}$, there is no detectable binding at that concentration of NaCl. In manganese-containing solutions where sodium chloride is replaced with 100 mM $CaCl_2$ or 100 mM $MgCl_2$, the $K_d$ of MntR rises to 550 ± 50 and 4000 ±1000 nM, respectively. These increases in $K_d$ are expected due to the enhanced competition of divalent cations for electrostatic interactions with DNA relative to monovalent ions (*39*, *40*). When no $Mn^{2+}$ is added to these solutions, MntR binds the fluoresceinated DNA with a $K_d$ of 1260 ± 310 nM in 100 mM $CaCl_2$, but no binding is observed in 100 mM $MgCl_2$ (Figure 6). Calcium is capable of activating MntR for DNA binding, but magnesium is not. The increased $K_d$ observed in the absence of $Mn^{2+}$, 1260 vs 550 nM, indicates that $Ca^{2+}$ fails to promote the fully activated conformation of MntR or that only about 50% of MntR dimers are in the activated conformation at 100 mM $CaCl_2$.

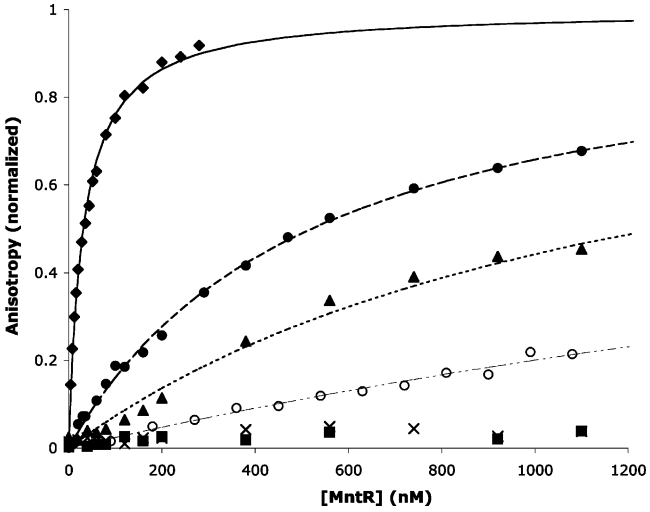


FIGURE 6: Normalized anisotropy vs the concentration of MntR in solutions containing 1 nM fluoresceinated DNA and (◆) 300 mM NaCl and 1 mM $Mn^{2+}$, (●) 100 mM $CaCl_2$ and 1 mM $Mn^{2+}$, (▲) 100 mM $CaCl_2$ without manganese, (○) 100 mM $MgCl_2$ with 1 mM $Mn^{2+}$, (×) 100 mM $MgCl_2$ without $Mn^{2+}$, and (■) 300 mM NaCl without $Mn^{2+}$. Curves were fit to the data assuming a 1:1 binding stoichiometry between the MntR dimer and DNA. The titration data taken from solutions without $Mn^{2+}$ in 300 mM NaCl and 100 $MgCl_2$ are normalized to the full signal observed in the presence of manganese.

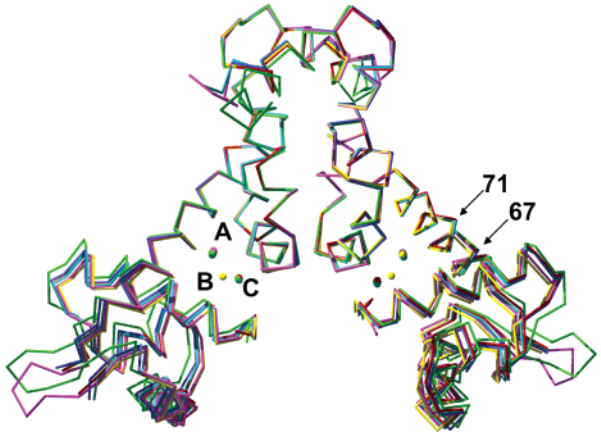


FIGURE 7: Overlay of the $C_\alpha$ backbone traces of the MntR complexes, superimposing residues 75−130 of both subunits. Conformer AB of the MntR·$Mn^{2+}$ complex is in yellow, conformer AC of the MntR·$Mn^{2+}$ complex is in blue, the MntR·$Mn^{2+}$ complex found in hexagonal crystals, also conformer AC, is in green, the MntR·$Cd^{2+}$ complex is in red, the MntR·$Ca^{2+}$ complex is in cyan, and the MntR·$Zn^{2+}$ complex is in magenta. The A, B, and C positions are labeled in the left subunit and the $C_\alpha$ positions of residues 67 and 71, representing the region where interdomain motion is *c*.

## DISCUSSION

MntR is activated by the formation of a binuclear metal ion complex at the interface of its DNA-binding and dimerization domains (*28*; Figure 1). The importance of the metal-binding geometry is illustrated by the modification of the metal-binding residue Asp8 to methionine. This substitution leads to a protein that binds a single metal ion per subunit and has reduced specificity for metal ion effectors and lower affinity for DNA (*15*, *17*). The goal of the present study is to understand how the intact binuclear complex confers metal ion specificity to MntR. Previous structural work implicated ionic size and the capacity to accept an expanded coordination geometry as key attributes of manganese as an activating metal. The results obtained here present a more complex view of metal ion binding by MntR but support the earlier conclusions. Also, they provide strong evidence that each metal-binding site in the binuclear complex has a distinct role in the metal-selective activation of MntR.

Unexpectedly, the structures reported here reveal two significantly different conformations, labeled AB and AC, for metal ion binding to MntR. The interconversion between the two conformers requires a shift in the position of the B/C $Mn^{2+}$ by 2.5 Å as well as reorganization of the bridging ligands. Otherwise, the same set of residues contributes to metal binding in both conformations, and the coordination geometries at both metals remain roughly constant in both conformations. The only obvious environmental differences are temperature, the protein−protein contacts that derive from crystal packing, and the conformational differences that permit those contacts. MntR displays backbone flexibility at the base of helix α4, including residues 66−71, that allows independent motion of the DNA-binding domains with respect to the dimerization domains, not unlike a pair of calipers (Figure 7). In the hexagonal crystal form, the MntR dimer is expanded, and the separation between recognition helices is 3 Å greater than that observed in monoclinic crystals at 100 K. Metal-binding residues Asp8 and Glu11 are on the N-terminal helix of MntR and move in concert with the rest of the DNA-binding domain, shifting in position by over 1.0 Å between the two crystal forms. Within monoclinic crystals of MntR·$Mn^{2+}$ residues Asp8 and Glu11 shift roughly 0.5 Å upon cooling (Figure 2D), perhaps in response to the decrease in unit cell volume that takes place upon cooling (*41*, *42*).

Precedent exists for the coupling of backbone movement to metal ion binding conformation. The designed metalloprotein L13G-DF1 binds a binuclear complex of manganese in two distinct conformations depending on the position of the protein in the asymmetric unit (*43*). A 0.7 Å shift in the positions of helices contributing metal-binding residues leads to displacement of a bridging solvent molecule and an increased distance between $Mn^{2+}$ ions, from 3.3 to 4.2 Å. The similarity of the conformational shift seen in L13G-DF1 and that observed in MntR is striking and has not to our knowledge been previously observed in a naturally occurring protein. Ultimately, the functionally important contacts that are made by MntR−metal ion complexes to elicit repression will only occur on cognate DNA. Recent work with the OhrR repressor from *B. subtilis* (*44*) reveals a protein that is capable of adapting significantly different "activated" conformations in the presence and absence of DNA. In the case of MntR, additional structural changes in the winged helix−turn−helix motifs and consequently in the metal-binding site are likely to be induced by DNA binding.

Other influences on the conformation of metal ion binding by MntR should not, however, be ruled out. Crystal packing cannot be definitively assigned as the cause of conformational changes seen in the coordination of manganese, though it may be permissive of such changes. The hexagonal packing geometry may disfavor conformer AB, and in other environments, it would predominate at low temperature. Simple thermodynamics may account for the appearance of the AB

conformation at low temperature in monoclinic crystals. For example, the coordination number at the metal sites of both manganese and iron superoxide dismutases is sensitive to temperature in solution (*45*, *46*). Likewise, the equilibrium between conjugate acids and bases can vary significantly with temperature. An early study by Keilin and Hartree (*47*) showed that the protonation state of the aquo ligand in methemoglobin is sensitive to temperature. Given the known sensitivity of bridging hydroxo ligands to pH in other manganese-binding proteins (*37*) and the sensitivity of buffer p$K_a$ to temperature change (*48*, *49*), it may be that cooling crystals of the MntR·$Mn^{2+}$ complex leads to a more basic environment and a more acidic water ligand, favoring the AB conformation.

The conformational shift in manganese binding observed in MntR provides an unusual view into the plasticity of metal ion binding by a regulatory protein and is an excellent reminder of the dynamic nature of protein systems. While it is somewhat surprising to see a >2 Å shift in metal ion position during the cooling process, a conformational change of this magnitude is consistent with observations in other proteins and current understanding of the flash-cooling process used in protein crystallography (*41*, *42*). Future studies, performed in solution, may be helpful in confirming a predominant conformation of manganese binding in MntR and specify which environmental influence(s) are responsible for the conformational shift observed in monoclinic crystals of MntR·$Mn^{2+}$. Additionally, structural studies of MntR bound to DNA will be especially useful in identifying the functional conformation(s) of the MntR·$Mn^{2+}$ complex. However, the additional structural information reported here on other metal ions complexed with MntR helps to describe the role of metal ion coordination in activating the protein for DNA binding.

The MntR·$Cd^{2+}$ complex provides additional insight into the active structure of the protein−metal complex. Data from in vivo and in vitro studies indicate that $Cd^{2+}$ activates MntR similarly to manganese (*8*, *16*, *17*). The dissociation constant of MntR·$Cd^{2+}$ from DNA is comparable to that observed with MntR·$Mn^{2+}$, and the ITC data reported here show that $Mn^{2+}$ and $Cd^{2+}$ bind with comparable affinity and stoichiometry to MntR. The binuclear cadmium complex is closest in overall structure to the AC conformation of the MntR·$Mn^{2+}$ complex (Figure 3A). Since the conformation of cadmium binding is insensitive to temperature, and so closely resembles the conformation of manganese binding observed at room temperature from pH 6.5 to pH 8.5, and in the hexagonal crystal form, it is reasonable to evaluate the AC conformation as a physiologically relevant metal-binding geometry in MntR. In the original structural analysis of MntR, the distorted hexacoordinate geometry of the A site with an additional weak metal−ligand interaction (~2.6 Å) was hypothesized to be the origin of manganese specificity. That hypothesis is consistent with the current models. As in conformer AB, both structures of the MntR·$Mn^{2+}$ complex solved from data collected at room temperature reveal seven ligands in close proximity to the A-site $Mn^{2+}$ (Table 3). The coordinate error associated with these structures and the positional disorder of the side chain of Glu11 in the cadmium complex (Figure S1) make it impossible to conclusively argue for a strong seventh metal−ligand bond, but the distorted geometry created by the other six ligands makes such an interaction possible. Thus we conclude that the unusual geometry of site A is accommodating to both high-spin $Mn^{2+}$ and $Cd^{2+}$ (*50*, *51*), which lack ligand field stabilization of coordination geometry.

Calcium is also a closed-shell metal cation adaptable to distorted coordination geometries (*50*) and in fact binds analogously to cadmium and manganese, yet it is less able to activate MntR, as demonstrated by previous studies performed in solution (*8*, *16*). ITC data presented here show that manganese and cadmium bind in the micromolar range, while no binding is observed for calcium at similar concentrations. However, 100 mM $Ca^{2+}$, much too concentrated to have physiological relevance, does partially activate MntR. The crystals of the MntR complex with calcium grew at an even higher concentration of calcium (200 mM) than used in our fluorescence anisotropy studies. With a requirement for $Ca^{2+}$ concentrations in the range of 100 mM to achieve even 50% activation, MntR possesses a roughly $10^4$-fold preference for manganese over calcium.

The selectivity of MntR against $Ca^{2+}$ likely involves ligand selection as a source of discrimination. The Irving−Williams series predicts that calcium will bind less tightly to ligands than manganese, especially nitrogenous ligands (*52*). In support of this prediction, naturally evolved calcium-binding sites rarely, if ever, contain histidine ligands as found in the MntR-binding site. In a recent survey of the RCSB Protein Data Bank by Lim and co-workers (*53*), it was found that of 260 ligands to manganese ions, 10.8% are histidine side chains, while among 437 ligands to calcium ions found in proteins, none are histidine. Thus ligand selection may play an important role in selectivity. The apparent aversion of $Ca^{2+}$ for nitrogen-containing sites enables substantial selectivity between the two metal ions, especially in vivo where the concentration of intracellular calcium in bacteria is generally submicromolar (*54*).

The value of ligand selection in discriminating against calcium is unlikely to extend to other first row divalent transition metals, such as $Zn^{2+}$, which have preferences for protein ligands similar to those found in MntR. Yet iron, cobalt, nickel, and zinc all activate MntR less well than $Mn^{2+}$ (*8*, *16*). While selectivity against each metal cation likely results from chemical features unique to each, the selectivity against zinc provides an interesting case study. In the presence of 1 mM $Zn^{2+}$, the dissociation constant of MntR from DNA is 2 $\mu$M, quite high relative to the $K_d$ of roughly 10 nM measured in the presence of $Mn^{2+}$ and $Cd^{2+}$ (*16*). The activation of MntR is clearly selective for manganese and cadmium over zinc, despite comparable dissociation constants in the micromolar range, as determined by ITC.

Single-site binding of $Zn^{2+}$ by MntR provides insight into the mechanism by which metal-selective activation is achieved. Zinc can be distinguished from manganese by virtue of its small ionic radius, which is 0.88 Å in octahedral complexes and significantly smaller than the 0.97 Å measured for high-spin $Mn^{2+}$ (*38*). The smaller size of zinc favors a lower coordination number in the A site of MntR, which in turn disrupts the ligand positions around the B/C sites, preventing the binding of a second metal ion and blocking the full activation of MntR. In the case of zinc, the A site acts as a selectivity filter, controlling occupancy of the B/C sites responsible for activation of MntR for high-affinity binding to its operators.

Structural and biochemical studies of the D8M mutant of MntR support these distinct roles for the A and B/C sites (*17*, *28*). D8M binds only one manganese ion per subunit due to modification of a B/C-site ligand, Asp8, to a nonbinding methionine. Both the affinity of D8M for DNA and its specificity for metal ion effectors are diminished (*15*, *17*). Presumably, the disrupted B/C site in D8M negates the ability of the A site to act as an effective selectivity filter, since formation of a functional activation site is no longer under the control of the metal-binding geometry in the A site. Likewise, D8M cannot be fully activated for DNA binding in the absence of a second bound metal.

The correlation of single-site binding to diminished activity takes place without any substantial, observable perturbation to the overall conformation of MntR in the crystalline state. The distance between DNA recognition helices in the MntR·$Zn^{2+}$ complex is not atypical for a dimer in the monoclinic crystal form. However, comparison of the MntR·$Zn^{2+}$ complex to the other metal ion complexes of MntR reveals an unraveling of the N-terminus that is unique to the zinc complex (Figure 4). Perhaps this is due to electrostatic repulsion between Asp8 and the other negatively charged groups in the region. Recent studies in the Cohen laboratory (*17*) indicate that the structure of D8M is considerably less ordered than wild-type MntR, even in the presence of $Mn^{2+}$ and $Cd^{2+}$. Work with DtxR has likewise shown that the crystalline state can obscure dynamic motion that is present in solution (*55*). Thus, the MntR·$Zn^{2+}$ complex may be considerably more flexible than the crystal structure reveals.

These results, coupled to the structures of cadmium and calcium bound to MntR, present a consistent picture of the selectivity of MntR for metal ion effectors. The three metal ions forming a binuclear complex, $Mn^{2+}$, $Ca^{2+}$, and $Cd^{2+}$ have relatively large ionic radii (0.97, 1.14, and 1.04 Å, respectively; *38*) and a capacity to adopt expanded coordination geometries (*50*, *51*). As a result, each metal ion can bind in the A site in such a way to orient residues appropriately for the second metal-binding site. Surprisingly, manganese can bind in one of two sites, either 3.3 or 4.4 Å distant from the A-site metal, but the principle of the A site acting as an activation filter holds. Calcium is a poor activator of MntR because it has low affinity for the A site, and zinc is unable to activate MntR because it fails to adopt the correct coordination geometry in that site. It is risky to extend these observations to other metal ions, since additional factors may come into play, but it is worth re-emphasizing that, among the divalent first row transition metal ions in octahedral environments, high-spin $Mn^{2+}$ has the largest ionic radius (*38*), and $Mn^{2+}$ is unusually flexible with respect to its coordination geometry (*51*). Thus, the selectivity of MntR for $Mn^{2+}$ over $Fe^{2+}$ as observed in vivo and in vitro (*8*, *15*, *17*) may be based on the geometry and size in the metal-binding sites. By extension, the somewhat surprising affinity of $Cd^{2+}$ for manganese-binding sites in proteins may be ascribed to the overall size of these sites and the capacity of $d^{10}$ $Cd^{2+}$ to adopt a variety of geometries (*51*).

MntR provides a unique illustration of how a binuclear metal complex may be used to moderate selectivity for metal ion effectors and activation for DNA binding. To our knowledge, ZntR is the only other metalloregulatory protein that has been seen to bind two effector ions ($Zn^{2+}$) in a binuclear complex (*21*), though several metalloregulatory proteins are known to bind multiple metal ions per subunit. Some, such as the ferric uptake regulator (Fur) of *E. coli* and the CadC regulator of *Staphylococcus aureus*, bind two different metal ions per subunit, with one metal ion ($Zn^{2+}$ in both of these cases) serving a structural role (*56*, *57*). A second regulatory site possesses the required selectivity for the cognate metal ion ($Fe^{2+}$ for Fur and either $Cd^{2+}$, $Pb^{2+}$, or $Zn^{2+}$ for CadC) and imparts allosteric changes that affect DNA binding. Members of the DtxR/MntR family bind two identical metal ions as effector ions in two distinct sites. DtxR has an ancillary site that is required for complete activation of the protein following binding of the iron(II) ion to the so-called primary site (*26*, *27*), though it is unclear if there is any communication between the sites responsible for metal-binding specificity. MntR is distinctive in coordinating two metal ion effectors in a binuclear complex at the interface of the DNA-binding and dimerization domains and in mediating a specific allosteric response to its cognate ion(s) through the intimate interaction of the two metal-binding sites.

Despite the revealing evidence presented here, significant uncertainties remain. Further study is required to confirm the physiological relevance of either or both metal-binding conformations of the MntR·$Mn^{2+}$ complex in DNA-binding activity. The conversation between the conformation of manganese binding and the positions of the DNA-binding domains may provide a means of adjusting the affinity of MntR to its cognate operators. Cocrystals of MntR bound to duplex DNA will be valuable in addressing those issues, and spectroscopic studies will be helpful in identifying the $Mn^{2+}$-binding conformation(s) present in solution.

## ACKNOWLEDGMENT

The authors thank Professor Seth Cohen for helpful conversations. Portions of this research were carried out at the Stanford Synchrotron Radiation Laboratory and the Advanced Light Source, national user facilities operated by Stanford University and Lawrence Berkeley National Laboratory on behalf of the U.S. Department of Energy, Office of Basic Energy Sciences. The SSRL Structural Molecular Biology Program and Berkeley Center for Structural Biology are supported in part by the Department of Energy, Office of Biological and Environmental Research, and by the National Institutes of Health, National Center for Research Resources, Biomedical Technology Program, and the National Institute of General Medical Sciences.

## SUPPORTING INFORMATION AVAILABLE

Omit electron density maps for the MntR·$Cd^{2+}$ complex showing two possible conformations for the interaction of Glu11 with the A-site cadmium ion. This material is available free of charge via the Internet at http://pubs.acs.org.

## REFERENCES

1. Pecoraro, V. (1999) Recent advances in the understanding of the biological chemistry of manganese, *Curr. Opin. Chem. Biol. 3*, 182−187.
2. Dismukes, G. C., Klimov, V. V., Baranov, S. V., Kozlov, Y. N., DasGupta, J., and Tyryshkin, A. (2001) The origin of atmospheric oxygen on Earth: The innovation of oxygenic photosynthesis, *Proc. Natl. Acad. Sci. U.S.A. 98*, 2170−2175.

3. Weisiger, R. A., and Fridovich, I. (1973) Superoxide dismutase: organelle specificity, *J. Biol. Chem. 248*, 3582−3592.
4. Jakubovics, N. S., and Jenkinson, H. F. (2001) Out of the iron age: new insights into the critical role of manganese homeostasis in bacteria, *Microbiology (Reading, U.K.) 147*, 1709−1718.
5. Kehres, D. G., and Maguire, M. E. (2003) Emerging themes in manganese transport, biochemistry and pathogenesis in bacteria, *FEMS Microbiol. Rev. 27*, 263−290.
6. Zaharik, M. L., and Finlay, B. B. (2004) $Mn^{2+}$ and bacterial pathogenesis, *Front. Biosci. 9*, 1035−1042.
7. Olanow, C. W. (2004) Manganese-induced parkinsonism and Parkinson's disease, *Ann. N.Y. Acad. Sci. 1012*, 209−223.
8. Que, Q., and Helmann, J. D. (2000) Manganese homeostasis in *Bacillus subtilis* is regulated by MntR, a bifunctional regulator related to the diphtheria toxin repressor family of proteins, *Mol. Microbiol. 35*, 1454−1468.
9. Guedon, E., Moore, C. M., Que, Q., Wang, T., Ye, R. W., and Helmann, J. D. (2003) The global transcriptional response of *Bacillus subtilis* to manganese involves the MntR, Fur, TnrA and $\sigma^B$ regulons, *Mol. Microbiol. 49*, 1477−1491.
10. Patzer, S. I., and Hantke, K. (2001) Dual repression by $Fe^{2+}$-Fur and $Mn^{2+}$-MntR of the *mntH* gene, encoding an NRAMP-like $Mn^{2+}$ transporter in *Escherichia coli*, *J. Bacteriol. 183*, 4806−4813.
11. Schmitt, M. P. (2002) Analysis of a DtxR-like metalloregulatory protein, MntR, from *Corynebacterium diphtheriae* that controls expression of an ABC metal transporter by an $Mn^{2+}$-dependent mechanism, *J. Bacteriol. 184*, 6882−6892.
12. Horsburgh, M. J., Wharton, S. J., Cox, A. G., Ingham, E., Peacock, S., and Foster, S. J. (2002) MntR modulates expression of the PerR regulon and superoxide resistance in *Staphylococcus aureus* through control of manganese uptake, *Mol. Microbiol. 44*, 1269−1286.
13. Ando, M., Manabe, Y. C., Converse, P. J., Miyazaki, E., Harrison, R., Murphy, J. R., and Bishai, W. R. (2003) Characterization of the role of the divalent metal ion-dependent transcriptional repressor MntR in the virulence of *Staphylococcus aureus*, *Infect. Immun. 71*, 2584−2590.
14. Ikeda, J. S., Janakiraman, A., Kehres, D. G., Maguire, M. E., and Slauch, J. M. (2005) Transcriptional regulation of *sitABCD* of *Salmonella enterica* serovar Typhimurium by MntR and Fur, *J. Bacteriol. 187*, 912−922.
15. Guedon, E., and Helmann, J. D. (2003) Origins of metal ion selectivity in the DtxR/MntR family of metalloregulators, *Mol. Microbiol. 48*, 495−506.
16. Lieser, S. A., Davis, T. C., Helmann, J. D., and Cohen, S. M. (2003) DNA-binding and oligomerization studies of the manganese(II) metalloregulatory protein MntR from *Bacillus subtilis*, *Biochemistry 42*, 12634−12642.
17. Golynskiy, M. V., Davis, T. C., Helmann, J. D., and Cohen, S. M. (2005) Metal-induced structural organization and stabilization of the metalloregulatory protein MntR, *Biochemistry 44*, 3380−3389.
18. Himeno, S., Yanagiya, T., Enomoto, S., Kondo, Y., and Imura, N. (2002) Cellular cadmium uptake mediated by the transport system for manganese, *Tohoku J. Exp. Med. 196*, 43−50.
19. Pennella, M. A., and Giedroc, D. P (2005) Structural determinants of metal selectivity in prokaryotic metal-responsive transcriptional regulators, *Biometals 18*, 413−428.
20. Schreiter, E. R., Sintchak, M. D., Guo, Y., Chivers, P. T., Sauer, R. T., and Drennan, C. L. (2003) Crystal structure of the nickel-responsive transcription factor NikR, *Nat. Struct. Biol. 10*, 794−799.
21. Changela, A., Chen, K., Xue, Y., Holschen, J., Outten, C. E., O'Halloran, T. V., and Mondragon, A. (2003) Molecular basis of metal-ion selectivity and zeptomolar sensitivity by CueR, *Science 301*, 1383−1387.
22. Tottey, S., Harvie, D. R., and Robinson, N. J. (2005) Understanding how cells allocate metals using metal sensors and metallochaperones, *Acc. Chem. Res. 38*, 775−783.
23. Qiu, X., Verlinde, C. L. M. J., Zhang, S., Schmitt, M. P., Holmes, R. K., and Hol, W. G. J. (1995) Three-dimensional structure of the diphtheria toxin repressor in complex with divalent cation co-repressors, *Structure 3*, 87−100.
24. White, A., Ding, X., vanderSpek, J. C., Murphy, J. R., and Ringe, D. (1998) Structure of the metal-ion-activated diphtheria toxin repressor/*tox* operator complex, *Nature 394*, 502−506.
25. Feese, M. D., Ingason, B. P., Goranson-Siekierke, J., Holmes, R. K., and Hol, W. G. J. (2001) Crystal structure of the iron-dependent regulator from *Mycobacterium tuberculosis* at 2.0 Å resolution reveals the Src homology domain 3-like fold and metal binding function of the third domain, *J. Biol. Chem. 276*, 5959−5966.
26. Spiering, M. M., Ringe, D., Murphy, J. R., and Marletta, M. A. (2003) Metal stoichiometry and functional studies of the diphtheria toxin repressor, *Proc. Natl. Acad. Sci. U.S.A. 100*, 3808−3813.
27. Rangachari, V., Marin, V., Bienkiewicz, E. A., Semavina, M., Guerrero, L., Love, J. F., Murphy, J. R., and Logan, T. M. (2005) Sequence of ligand binding and structure change in the diphtheria toxin repressor upon activation by divalent transition metals, *Biochemistry 44*, 5672−5682.
28. Glasfeld, A., Guedon, E., Helmann, J. D., and Brennan, R. G. (2003) Structure of the manganese-bound transporter of *Bacillus subtilis*, *Nat. Struct. Biol. 10*, 562−657.
29. Leslie, A. G. W. (1992) Recent changes to the MOSFLM package for processing film and image plate data, *Joint CCP4 + ESF-EAMCB Newsletter on Protein Crystallography 26*.
30. Pflugrath, J. W. (1999) The finer things in X-ray diffraction data collection, *Acta Crystallogr. D55*, 1718−1725.
31. Bailey, S. (1994) The CCP4 suite: programs for protein crystallography, *Acta Crystallogr. D50*, 760−763.
32. Brünger, A. T., Adams, P. D., Clore, G. M., Delano, W. L., Gros, P., Grosse-Kunstleve, R. W., Jiang, J.-S., Kuszewski, J., Nilges, M., Pannu, N. S., Read, R. J., Rice, L. M., Simonson, T., and Warren, G. L. (1998) Crystallography & NMR System: a new software suite for macromolecular structure determination, *Acta Crystallogr. D54*, 905−921.
33. Stevenson, C. E. M., Tanner, A., Bowater, L., Bornemann, S., and Lawson, D. M. (2004) SAD at home: solving the structure of oxalate decarboxylase with the anomalous signal from manganese using X-ray data collected on a home source, *Acta Crystallogr. D60*, 2403−2406.
34. Laskowski, R. A., MacArthur, M. W., Moss, D. S., and Thornton, J. M. (1993) *PROCHECK*: a program to check the stereochemical quality of protein structures, *J. Appl. Crystallogr. 26*, 283−291.
35. Lundblad, J. R., Laurance, M., and Goodman, R. H. (1996) Fluorescence polarization analysis of protein-DNA and protein-protein interactions, *Mol. Endocrinol. 10*, 607−612.
36. Brennan, R. G. (1993) The winged-helix DNA-binding motif: Another helix-turn-helix takeoff, *Cell 74*, 773−776.
37. Wilce, M. C. J., Bond, C. S., Dixon, N. E., Freeman, H. C., Guss, J. M., Lilley, P. E., and Wilce, J. A (1998) Structure and mechanism of a proline-specific aminopeptidase from *Escherichia coli*, *Proc. Natl. Acad. Sci. U.S.A. 95*, 3472−3477.
38. Shannon, R. D. (1976) Revised effective ionic radii and systematic studies of interatomic distances in halides and chalcogenides, *Acta Crystallogr. A32*, 751−767.
39. Li, A. Z., Huang, H., Re, X., Qi, L. J., and Marx, K. A. (1998) A gel electrophoresis study of the competitive effects of monovalent counterion on the extent of divalent counterions binding to DNA, *Biophys. J. 74*, 964−973.
40. Record, M. T., deHaseth, P. L., and Lohman, T. M. (1977) Interpretation of monovalent and divalent cation effects on the *lac* repressor-operator interaction, *Biochemistry 16*, 4791−4796.
41. Juers, D. H., and Matthews, B. W. (2001) Reversible lattice repacking illustrates the temperature dependence of macromolecular interactions, *J. Mol. Biol. 311*, 851−862.
42. Halle, B. (2004) Biomolecular cryocrystallography: Structural changes during flash cooling, *Proc. Natl. Acad. Sci. U.S.A. 101*, 4793−4798.
43. DeGrado, W. F., Costanzo, L. D., Geremia, S., Lombardi, A., Pavone, V., and Randaccio, L. (2003) Sliding helix and change of coordination geometry in a model di-Mn(II) protein, *Angew. Chem., Int. Ed. 42*, 417−420.
44. Hong, M., Fuangthong, M., Helmann, J. D., and Brennan, R. G. (2005) Structure of an *ohrR-ohrA* operator complex reveals the DNA binding mechanism of the MarR family, *Mol. Cell 20*, 131−141.
45. Whittaker, M. M., and Whittaker, J. W. (1996) Low-temperature thermochromism marks a change in coordination for the metal ion in manganese superoxide dismutase, *Biochemistry 35*, 6762−6770.
46. Renault, J. P., Morgenstern-Badarau, I., and Piccioli, M. (1999) Thermochromic conformational change of *Methanobacterium thermoautotrophicum* iron superoxide dismutase, *Inorg. Chem. 38*, 614−615.

47. Keilin, D., and Hartree, E. F. (1949) Effect of low temperature on the absorption spectra of haemoproteins: with observations on the absorption spectrum of oxygen, *Nature 164*, 254−259.
48. Good, N. E., Winget, G. D., Winter, W., Connolly, T. N., Izawa, S., and Singh, R. M. M. (1966) Hydrogen ion buffers for biological research, *Biochemistry 5*, 467−477.
49. Hoa, G. H. B., and Douzou, P. (1973) Ionic strength and protonic activity of supercooled solutions used in experiments with enzyme systems, *J. Biol. Chem. 248*, 4649−4654.
50. Harding, M. M. (2000) The geometry of metal−ligand interactions relevant to proteins. II. Angles at the metal atom, additional weak metal-donor interactions, *Acta Crystallogr. D56*, 857−867.
51. Holloway, C. E., and Melnik, M. (1995) Cadmium coordination compounds: classification and analysis of crystallographic and structural data, *Main Group Met. Chem. 18*, 451−585.
52. Sigel, H., and McCormick, D. B. (1970) On the discriminating behavior of metal ions and ligands with regard to their biological significance, *Acc. Chem. Res. 3*, 301.
53. Dudev, T., and Lim, C. (2003) Principles governing Mg, Ca, and Zn binding and selectivity in proteins, *Chem. Rev. 103*, 773−787.
54. Dominguez, D. C. (2004) Calcium signaling in bacteria, *Mol. Microbiol. 54*, 291−297.
55. Twigg, P. D., Parthasarathy, G., Guerrero, L., Logan, T. M., and Caspar, D. L. D. (2001) Disordered to ordered folding in the regulation of diphtheria toxin repressor activity, *Proc. Natl. Acad. Sci. U.S.A. 98*, 11259−11264.
56. Pohl, E., Haller, J. C., Mijovilovich, A., Meyer-Klaucke, W., Garman, E., and Vasil, M. L. (2003) Architecture of a protein central to iron homeostasis: crystal structure and spectroscopic analysis of the ferric uptake regulator, *Mol. Microbiol. 47*, 903−915.
57. Ye, J., Kandegedara, A., Martin, P., and Rosen, B. P. (2005) Crystal structure of the *Staphylococcus aureus* pI258 CadC Cd(II)/Pb(II)/Zn(II)-responsive repressor, *J. Bacteriol. 187*, 4214−4221.

BI0524215